VIII-Ⅱ-1. Project Research

Project 1

PR1 Application Studies on Effective Use of F-Elements

H. Yamana

Research Reactor Institute, Kyoto University

1. Objectives and Allotted Research Subjects

Studies on actinide nuclides with careful management are being more important for reprocessing, disposal, partitioning, and transmutation processes in the nuclear fuel cycle. Hot laboratory of KURRI is one of core facilities in Japan, in which actinides especially transuranic elements can be treated. The actinide studies are expanded for fundamental and application studies on f-elements. Allotted research subjects are as the followings.

ARS-1 Dissolution and precipitation behavior of actinides and radio nuclides.

ARS-2 Study on complexation of actinides in aqueous solutions (T. Sasaki *et al.*).

ARS-3 Dissolution behavior of actinides and FPs from irradiated nuclear materials (N. Sato *et al.*).

ARS-4 Systematic study on extraction characteristics of actinides (A. Shinohara *et al.*).

ARS-5 Fundamental and application studies on effective use of f-elements (Y. Ikeda *et al.*).

ARS-6 Study on chemical isotope effect of actinides and fission product elements (T. Fujii *et al.*).

ARS-7 Isotope separation by using microreactor (R. Hazama *et al.*).

ARS-8 Analysis of trace f-elements in volcanic samples (T. Shibata *et al.*).

ARS-9 Electrochemical study of uranium in pyrochemical reprocessing system (Y. Sakamura *et al.*).

ARS-10 XAFS analysis on halogenides containing actinides and FP elements (H. Matsuura *et al.*).

ARS-11 Spectroelectrochemical analysis of actinide ions in molten salts and hydrate melts (A. Uehara *et al.*)

ARS-12 Molecular dynamics simulation of molten salts containing f-elements (N. Ohtori *et al.*)

ARS-13 Fundamental study on electrolytic formation/dissolution of f-element compounds in molten salts (T. Goto *et al.*).

ARS-14 Absorption spectrophotometric study on metal ions in molten salts. (H. Sekimoto *et al.*)

ARS-15 Thermal and mechanical properties of actinides-containing ceramics (S. Yamanaka *et al.*).

ARS-16 Study on neutron capture cross sections of long-lived nuclides by activation method (S. Nakamura *et al.*).

2. Main Results and Contents

ARS-1 and 3 clarified dissolution behavior of actinides, FPs, and ^{14}C, which are generated by neutron irradiation of target materials, in aqueous solution. ARS-2 and 4 studied aqueous chemistry of actinides and FP elements. ARS-2 pointed out the important feature of the potential correlated with the behavior of agglomeration/ polymerization of Th. ARS-5 studied solvent extraction of ^{99m}Tc and ^{99}Mo. An effective separation of ^{99m}Tc was proposed. ARS-5, 9, and 12 studied the U chemistry in low temperature or room temperature melts. In ARS-7, coodination circumstance of $[EMI]_2[UO_2(NO_3)_4]$ in ionic liquids was studied by absorption spectrophotometry. In ARS-9, redox behavior of U at silicon electrode in LiCl-KCl melt was clarified by cyclic voltammetry. ARS-12 studied MD simulation for concentrated LiCl aqueous solutions containing uranyl chloride, and evaluated the local structure of U. ARS-6, 7, and 8 studied isotopic differences in Ca, Sr, and U in aqueous systems. ARS-6 studied intramolecular vibrations, which is important factor for isotope fractionation, of uranyl complexes. A correlation between the vibrational frequencies with ligand exchange at the equatorial plane was found. ARS-7 studied isotope fractionation of Ca. A possible fractionation of $^{48}Ca/^{40}Ca$ was found. ARS-8 studied precise isotopic analysis of Sr. Isotope dilution technique was demonstrated. ARS-10, 11, 13, and 14 studied the chemical behavior of FP elements (Nd and Zr), and structural material elements in molten salts, the results of which are to be dedicated to the development of nuclear fuel cycle or general industrial use. In ARS-10 and 14, electronic absorption spectra of Nd were measured. Effects of adding fluoride or borate were clarified. In ARS-11, redox behavior of Zr in LiCl-KCl eutectic salt bath was clarified by cyclic voltammetry. ARS-13 studied electrochemical behavior and liquid structures of molten alkaline chlorides containing Al. Raman spectra obtained were interpreted by using *ab initio* method. In ARS-15, thermal conductivity of Y_6UO_{12} was successfully obtained. In ARS-16, the thermal-neutron capture cross section of ^{243}Am was newly evaluated.

3. Summaries of the achievements

In this research, by using various unique facilities of KURRI for f-element research, new and characteristic chemical and nuclear physical data were obtained. These new information encompass solid chemistry, molten salt and solution chemistry, as well as nuclear reactions of f-elements. The results are useful either for scientific purpose or for technological purpose for nuclear science and general industry.

採択課題番号　25P1　ｆ－元素の有効利用に関わる基礎及び応用研究　　プロジェクト

（京大・原子炉）山名　元

PR1-1 Behaviour of C-14 Compounds Dissolved from Irradiated Metallic Materials

T. Kobayashi, K. Date, T. Uemura, Y. Matsuura, T. Sasaki, H. Moriyama[1], H. Yamana[1], T. Fujii[1], T. Fukutani[1] and R. Okumura[1]

Graduate School of Engineering, Kyoto University
[1]Research Reactor Institute, Kyoto University

INTRODUCTION:

Hull (Zircaloy) and end-piece (stainless steel) wastes categorized as Group 2 of TRU wastes contain an activated isotope C-14, which is mainly generated by the $^{14}N(n,p)^{14}C$ reaction in light water reactor. These wastes are planned to be disposed of in a deep underground repository. Special attention in the long-term safety assessment of the TRU waste is to be given for the behavior and speciation of C-14 released from neutron-activated materials to the repository conditions; the near-field, far-field and biosphere. However, the dissolution and reaction mechanism of C-14 at the surface of corroded metal is not sufficiently known yet [1,2]. One of reasons is due to few number of real samples, which could be prepared in commercial light water reactor.

The purpose of the present study is i) the preparation of simulated wastes of zirconium metal species containing C-14 by research reactor, and ii) the speciation of dissolved carbon compounds by using sequential separation method and high-performance liquid chromatography (HPLC).

EXPERIMENTS:

i) Production of C-14 in metal sample

The powder samples of zircaloy-4 and stainless steel SUS316L were heated at nitrogen gas atmosphere to absorb the nitrogen atoms into the samples. For the treatment of the surface oxidation, some samples were heated at ambient condition. About one gram of powder sample was sealed into a quartz tube in vacuo. The tube was inserted into the aluminum capsule and neutron-irradiated (5MWx3h) at the Kyoto University Reactor (KUR).

ii) Leaching test of materials

The sample was left for a few weeks to reduce the high radioactivity from short-lived nuclides. The powder sample was then suspended in 10 ml of NaOH solution (pH 12.5). After the aging time in the anaerobic condition at room temperature, a gaseous species of C-14 in the vessel was transferred to the ionization chamber by air-purging, and the radioactivity was measured (Fig. 1). To separately determine the fractions of inorganic and organic C-14 compounds, the nitric acid was added to collect inorganic species of C-14 from the aqueous phase to the alkaline trap, followed by adding $K_2S_2O_8/AgNO_3$ to oxidize organic species of C-14 in the same manner. The radioactivity of leached fractions after the above chemical treatment was measured by liquid scintillation counting (LSC).

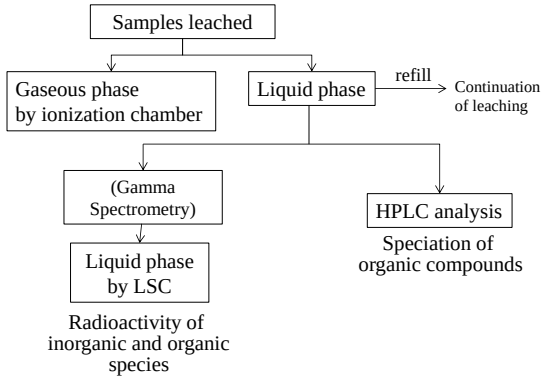

Fig. 1.
Analytical flow sheet of C-14 in the gaseous and liquid phases after leaching of irradiated samples.

RESULTS:

The dissolution amount of C-14 from the Zry-4 after 1 month was shown in Fig. 2. The quite low component of gaseous C-14 was not detected by ionization chamber. The apparent dissolution rate of aqueous species reached a plateau after 4 months. The rate of the surface-oxidized samples was found to be lower than that of non-oxidized ones, and the considerably lower organic component was dissolved. It is probably due to the difference of oxygen potential at the surface of oxidized and non-oxidized samples. By HPLC analysis, the major organic component was found to be lower carboxylic acid, such as formic and acetic acids.

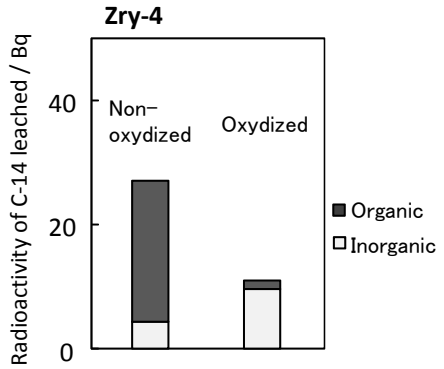

Fig. 2 Comparison of leached species from Zry-4 to NaOH solution, after 1 month at 25 ºC.

REFERENCES:

[1] T. Yamaguchi, S. Tanuma, I. Yasutomi, T. Nakayama, H. Tanabe, K. Katsurai, W. Kawamura, K. Maeda, H. Kitao, M. Saigusa, Proceedings of ICEM 99, September, Nagoya, Japan(1999).

[2] Second Progress Report on Research and Development for TRU Waste Disposal in Japan, JAEA-Review 2007-010, FEPC TRU-TR2-2007-01 (2007).

採択課題番号 25P1-1 アクチニド元素および放射性核種の溶解沈殿反応に関する研究 プロジェクト
（京大院・工）小林 大志、伊達 海斗、上村 拓也、佐々木 隆之
（京大・原子炉）森山 裕丈、山名　元、藤井 俊行、福谷　哲、奥村　良

PR1-2 Zeta Potential and Apparent Solubility of Thorium-Humic Substance Complex

T. Sasaki, Y. Matsuura, T. Koukami, T. Kobayashi, H. Moriyama[1], H. Yamana[1] and T. Fujii[1]

Graduate School of Engineering, Kyoto University
[1]Research Reactor Institute, Kyoto University

INTRODUCTION:

The reaction of humic substances (HSs) with tetravalent actinide ions is competitive with the hydrolysis reaction in which the tetravalent ions form polynuclear, colloidal species and hydroxide precipitates. Hence the resulting soluble species and solid phase compositions are determined by the balance of the hydrolysis and ligand-complexation reactions. The apparent solubility of thorium in the presence of organic ligand after filtration has been investigated as a function of the proton concentration (pHc). In the presence of artificial simple carboxylic ligand, few Th colloidal species larger than 2 nm were observed, and the solubility appeared to be controlled by thorium-OH-carboxylate solid phases [1]. Th solubility in the presence of fumaric acid was similar to that in the presence of succinic acid, whereas no solid phase was observed in the presence of maleic acid under pH 4. Thus, organic ligand having strong interaction with Th(IV) is thought to play an important role in the migration and a dicarboxylic acid which coordinates with a chelate configuration, can be considered as a model substance of humic substances in groundwater.

The present study focuses on the relationship between apparent solubility of Th-HA (purified Aldrich humic acid) species determined by sequential filtration with different pore-sized filters, and zeta-potential of supernatant with some colloids. The potential could be correlated with the behavior of agglomeration/polymerization of thorium in the presence of HA and matrix ions, and with the temperature effect.

EXPERIMENTS:

Solubility batch samples with Th in the presence of HA were prepared in an argon glove box by oversaturation approach. Shortly, sample solutions were obtained by diluting the Th stock solution with perchloric acid, divided into 10 mL aliquots in polypropylene tubes, and the pH conditions were adjusted by adding aliquots of $HClO_4$ or NaOH solution. Initial Th concentrations were around 10^{-4} M, and the ionic strength was fixed at I = 0.1 and 1 M by adding appropriate amounts of $NaClO_4$. The samples were aged for given periods of time. Then, the supernatants filtered with different pore-sized membranes (Microcon NMWL 3 kDa (2 nm), and Dismic 0.45 μm). The Th concentration in the filtrates was determined by ICP-MS (HP4500, Hewlett Packard).

The zeta potential of samples was determined by using a Malvern Instruments Zetasizernano ZS used laser Doppler velocimetry to determine the electrophoretic mobility of suspended matter including colloid.

RESULTS:

In the initial concentration of [HA]=5x10^{-3} eq/L and [Th]= 5x10^{-4} M at I = 1, over 90% Th species could be filtered out by 0.45 μm filter at the neutral pH region, and the apparent solubility after filtration through 3 kDa membrane was much lower than that through 0.45 μm filter, indicating the coagulation and size distribution of HS complexes (Fig. 1). At I = 0.1, on the other hand, the smaller species between 3 kDa and 0.45 μm filters was considered to be dominant species. The growth of Th-HS complex in size at I = 1 might be caused by the higher concentration of Na^+ ion.

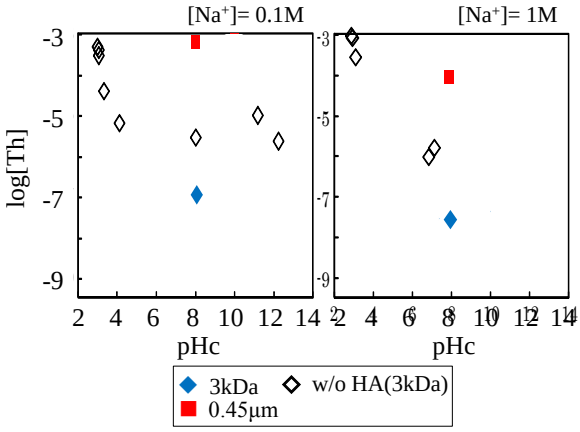

Fig. 1.
Apparent solubility of Th in the presence/absence of HA under different I at 25C aft 2 months.

Figure 2 shows an example of zeta potential of Th-HA complex. Higher and constant potential values around -20mV were observed at I = 1 due to the charge neutralization of Th-HA complex by Na^+ ion.

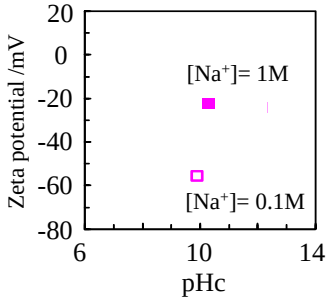

Fig. 2. Zeta potential of Th-HA complex in the excess amount of humic acid to Th.

REFERENCES:

[1] T. Kobayashi, T. Sasaki, I. Takagi, H. Moriyama, "Solubility of Thorium(IV) in the Presence of Oxalic and Malonic Acids," J. Nucl. Sci. Technol., 46, 1085-1090 (2009).

採択課題番号 25P1-2　アクチニド元素の水溶液内錯生成反応に関する研究　　プロジェクト
（京大院・工）佐々木 隆之、松浦由佳、鴻上 貴之、小林 大志
（京大・原子炉）森山 裕丈、山名　元、藤井 俊行

PR1-3 Dissolution Behavior of Actinides and FPs in Spent Nuclear Fuel

N. Sato, A. Kirishima, Y. Fukuda, T. Sasaki[1], T. Kobayashi[1], A. Uehara[2], T. Fujii[2], K. Takamiya[2] and H. Yamana[2]

Institute of Multidisciplinary Research for Advanced Materials, Tohoku University
[1]Graduate School of Engineering, Kyoto University
[2]Research Reactor Institute, Kyoto University

INTRODUCTION:

After the station black out of Tokyo Electric Power Company (TEPCO) Fukushima Daiichi Nuclear Power Station, thousands of tons of seawater for cooling the high temperature reactor cores was injected. Under high temperature condition in the pressure vessel, several kinds of FPs and TRU were possibly released into the cooling water mixed with seawater and the air from the melted core and its fine debris which might be reacted with a certain amount of zirconium alloy of the cladding of the fuel and/or its oxide. Simulating the radionuclide behavior in the surface seawater will be helpful to analyze the forthcoming analysis data about the contents of minor FPs and TRU in contaminated water, and to manage associated secondary wastes.

First, the possible fuel debris composed of uranium and zirconium oxides as main constituents in the reactor was prepared by heat treatment in reductive or oxidative conditions. Then the dissolution behavior of typical gamma-ray fission products and neutron activated nuclides as well as uranium in solid solutions was investigated by neutron irradiation and following leaching in the non-filtrated seawater. Dissolution behavior of MA was also studied by the used of MA doped simulated fuel debris.

EXPERIMENTAL:

Three types of UO_2-ZrO_2 solid solution samples with Zr concentration of 10, 50 and 90 mol% were prepared by mechanochemical and heat treatments under reductive or oxidative atmosphere. The sample was vacuum-sealed in quartz tube and irradiated for 20 min using the pneumatic transferring system (Pn-2) at KUR. For reducing the high radioactivity of short-lived nuclides, the sample was left in glove box, and then suspended in 30 ml of fresh seawater from Minamisoma city, Fukushima. After the aging time in the atmospheric condition at R.T., a 10 mL of supernatant was transferred to new sample tube after filtration with 0.45 μm (Advantec) or 3 kDa (Microcon, Millipore) membranes, followed by evaporation of the seawater at 363 K in order to prepare a solidified point-like source. For MA doped sample, similar preparation techniques were applied by using U_3O_8 powder doped with Np-237, Am-243. Gamma- and alpha ray spectrometry were performed using a Ge detector (GMX15P4, Ortec) and Si-detector (7401, Camberra) to determine the nuclides leached.

RESULTS:

After the separation of filtrates from the irradiated sample through the 0.45μm membrane, the gamma-ray spectrum of the filtrate was measured. Figure 1 shows the gamma-ray spectrum of the filtrate obtained at 160 days later after the irradiation. The gamma-rays from Th-234, the daughter of U-238 were observed as well as that of U-235 suggesting the dissolution of fuel material. Gamma-rays from FP nuclides such as Cs-137 at 662, Ru-103 at 497, and Zr-95 at 757 keV were also observed in the spectrum. This indicates the dissolution of FP elements in the seawater even at room temperature. Dissolution ratios of FP elements in the oxidative samples seem to be high compared with those in the reductive ones. In the case of MA doped samples, dissolution ratios of MA elements were very low as well as uranium, though some of them slightly increased with increasing leaching time.

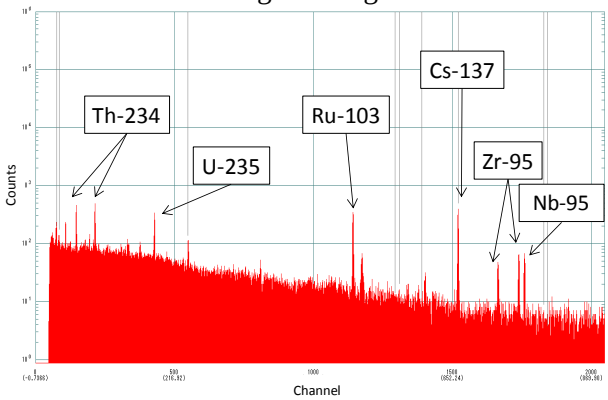

Fig.1 Gamma ray spectrum of the filtrate. (160 days after irradiation)

SUMMARY:

In this study, dissolution behavior of FP and MA in the spent fuel into seawater was found to be affected by the oxidative or reductive condition of uranium and zirconium oxides. For the further study of fuel debris treatment, dissolution behavior of FP and MA in fuel debris shold aslo be discussed with different types of simulated debris containing other components such as metals and concrete.

採択課題番号 25P1-3　　使用済燃料中のアクチノイドおよび FP 元素の溶解挙動に関する研究　　プロジェクト
（東北大多元研）佐藤修彰、桐島　陽、福田祐平　（京大院工）佐々木隆之、小林大志
（京大・原子炉）上原章寛、藤井俊行、高宮幸一、山名　元

PR1-4 Preparation of ^{99m}Tc from ^{99}Mo of Low Specific Activity

Y. Hayashi, N. Takahashi, K. Nakai, H. Ikeda[1], K. Takamiya[2], Y. Kasamatsu and A. Shinohara

Graduate School of Science, Osaka University
[1]Graduate School of Medicine, Osaka University
[2]Research Reactor Institute, Kyoto University

INTRODUCTION: We applied chemical studies on Tc and Mo, homologues of superheavy elements, to nuclear medicine research. A radioisotope of ^{99m}Tc is one of the most important radioisotopes used for diagnostic radiopharmaceuticals today. Most of ^{99m}Tc are produced by the several nuclear reactors in the world. However, all those reactors using highly enriched ^{235}U fuel are aged more than 50 years, and thus their deteriorations are anticipated. Many alternative methods were developed for the production of ^{99m}Tc, as the ^{100}Mo(*p*, *2n*)^{99m}Tc and ^{100}Mo(*p*, *d*)^{99}Mo reactions[1] [2]. In our previous work, we tested to produce ^{99}Mo which is parent nuclide of ^{99m}Tc with spallation neutron reaction of ^{100}Mo(*n*, *2n*)^{99}Mo that has larger cross section than the proton induced reactions. The produced radioactivity of ^{99}Mo was 3 MBq/(μA h g) and this result suggested that enough radioactivities of ^{99}Mo for the medical use are able to be obtained with this method. However, the present specific radioactivity of ^{99}Mo produced by the ^{100}Mo(*n*, *2n*)^{99}Mo reaction is very low, and it is difficult for such a sample to purify ^{99m}Tc by the conventional alumina and PZC columns. In this work, we separated ^{99m}Tc from neutron-irradiated ^{nat}Mo sample by the solvent extraction with methyl ethyl ketone (MEK) and further purified ^{99m}Tc with the alumina column.

EXPERIMENTS: The chemical scheme applied to the present work is shown in Fig. 1. The low specific activity ^{99}Mo was prepared by mixing 40 g of $^{nat}MoO_3$ with 40 mg of thermal-neutron-irradiated MoO_3. The irradiation was performed by Pn-2 of Kyoto University Research Reactor (1 MW) in 20 min. The mixture was dissolved with 120 mL of 4 M sodium hydroxide solution, and a few drops of H_2O_2 (36 wt%) was added to equalize the valence of molybdenum ion. The ^{99m}Tc nuclide was extracted with 15 mL of MEK from the solution sample. After the evaporation of the MEK solution under reduced pressure, the sample was dissolved with a 2 mL of saline. The solution was passed through the neutral alumina column to remove the Mo species by adsorbing them on the column. Amount of impurities in the ^{99m}Tc solution were measured with ICP-MS and the yield of ^{99m}Tc was determined by gamma-ray measurement using a germanium semiconductor detector. Furthermore, the purified ^{99m}Tc was labeled into methylene diphosphonate (MDP).

RESULTS: As the results of measurement with ICP-MS, we found that only less than 10 ppb of Mo and Al coexist in the purified ^{99m}Tc solution. .No other impurities were also observed in gamma-ray spectrum (Fig.2), and this solution was satisfied with the demand of the United States Pharmacopeia (USP). The present yield of ^{99m}Tc was 75-90%, which is high comparably with that in Ref. [3]. It was found that sufficiently pure ^{99m}Tc for medical use was obtained by the present method using MEK and alumina column from the sample containing macro amount of ^{nat}Mo.

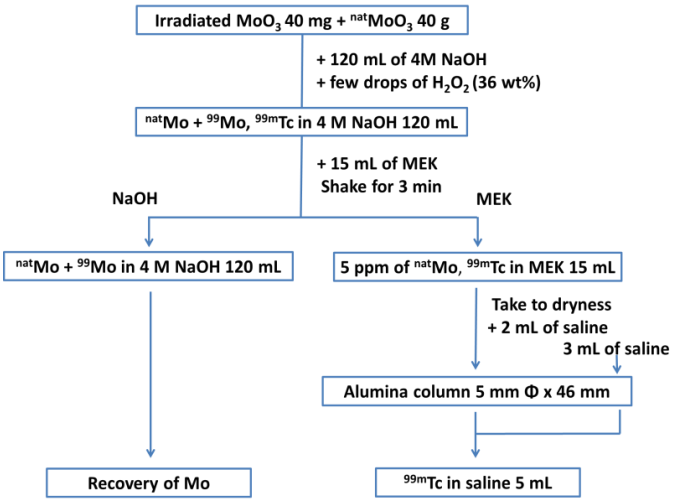

Fig. 1. Scheme for the separation of ^{99m}Tc from ^{nat}Mo and ^{99}Mo matrix.

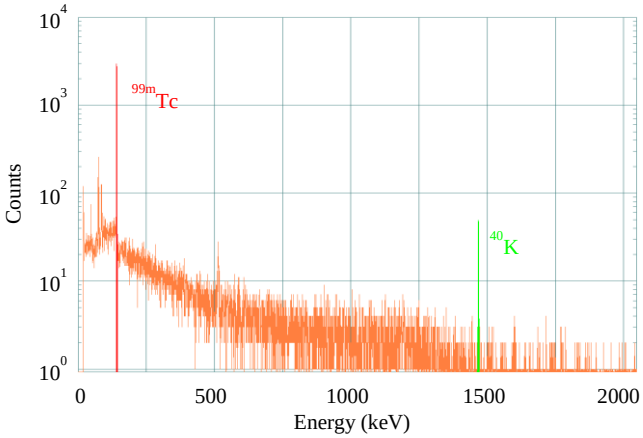

Fig. 2. Gamma-ray spectrum of purified ^{99m}Tc sample (3600 s).

REFERENCES:

[1] B. Scholten *et al.*, Appl. Radiat. Isot., **51** (1999) 69-90.
[2] K. Gagnon *et al.*, Nucl. Med. Biol., **38** (2011) 907-916.
[3] A. Kimura *et al.*, JAEA-Testing 2012-002 (2010).

採択課題番号 25P1-4　　重・超アクチノイド元素の抽出挙動　　プロジェクト
（阪大院・理）林　良彦、高橋成人、中井浩二、笠松良崇、篠原　厚、（阪大院・医）池田隼人、（京大炉）高宮幸一

PR1-5 Structural Studies of Uranyl Species in 1-Ethyl-3-Methylimidazolium Nitrate

K. Sasaki, M. Harada, T. Suzuki and Y. Ikeda

Research Laboratory for Nuclear Reactors, Tokyo Institute of Technology

INTRODUCTION: Uranyl trinitrato complex in non-aqueous solvents and in solid state has been known to exist as $[UO_2(NO_3)_3]^-$ with D_{3h} symmetry [1-3]. Uranyl nitrato complexes in ionic liquids (ILs) have also been examined using spectroscopic methods such as UV-visible, EXAFS, and so on [4-7]. Such studies have clarified that the uranyl nitrato complexes in ILs exist as $[UO_2(NO_3)_3]^-$ with D_{3h} symmetry. However, recently it was reported that $[DMI]_2[UO_2(NO_3)_4]$ (DMI =1,3-dimethylimidazolium) is obtained as a single crystal and that uranyl species exist as $[UO_2(NO_3)_4]^{2-}$ in [BMI][NO_3] (BMI = 1-butyl-3-methylimidazolium). In these complexes, the equatorial plane of uranyl moiety is coordinated by two bidentate and two unidentate nitrates [8, 9]. In the present study, to get more detail information on the structure of uranyl nitrato complexes, we have examined the structures of uranyl species in CH_3CN and [EMI][NO_3] dissolving $[EMI]_2[UO_2(NO_3)_4]$(EMI = 1-ethyl-3-methylimidazolium).

EXPERIMENTS: The $[EMI]_2[UO_2(NO_3)_4]$ complex was synthesized by adding four equivalent of $AgNO_3$ to $[EMI]_2[UO_2Cl_4]$ in CH_3CN, followed by filtration for removing AgCl and evaporation of CH_3CN. Sample solutions were prepared by dissolving $[EMI]_2[UO_2(NO_3)_4]$ complex into CH_3CN or [EMI][NO_3]. The UV-visible absorption spectra of solutions were measured by Shimadzu UV-3150 spectrophotometer. EXAFS measurements were carried out using PF BL27B at High Energy Accelerator Organization.

RESULTS: UV-visible absorption spectrum of sample solution prepared by dissolving $[EMI]_2[UO_2(NO_3)_4]$ complex(0.024 M, M = mol dm^{-3}) into CH_3CN was measured and found to be consistent with that of the $[UO_2(NO_3)_3]^-$ species with D_{3h} symmetry. We also measured the absorption spectral changes with the addition of [EMI][NO_3] (0.050, 0.10, 0.20, 0.50, 1.5 M) to the above CH_3CN solution dissolved $[EMI]_2[UO_2(NO_3)_4]$ (0.024 M). The results are shown in Fig. 1.The absorbance in the range of 420 to 440 nm is found to increase with appearance of isosbestic points at 465 and 469 nm. This phenomenon is similar to that reported by Ryan [2], i.e., the absorption spectra of CH_3NO_2 solutions dissolved $(C_2H_5)_4UO_2(NO_3)_3$ and $(C_2H_5)_4NNO_3$ showed the isosbestic points at 465.5 and 470.0 nm. From these results, it is proposed that the following equilibrium reaction exists in the present system.

$$[UO_2(NO_3)_3]^- + NO_3^- = [UO_2(NO_3)_4]^{2-},$$

Based on the absorption spectral changes, the equilibrium constant (K) was evaluated as 3.85 M^{-1}, which is in agreement with the data reported by Ryan, 4.74 M^{-1} [2].

Furthermore, we measured UV-visible absorption and EXAFS spectra of [EMI][NO_3] solution dissolved $[EMI]_2[UO_2(NO_3)_4]$ at 50 ºC. The UV-visible absorption spectrum (Fig. 1) was found to be consistent with that of [EMI][NO_3] dissolved $UO_2(NO_3)_2{\cdot}6H_2O$. From the EXAFS data, it was supported that the uranyl species in [EMI][NO_3] are present as $[UO_2(NO_3)_4]^{2-}$ and its equatorial plane is coordinated by two bidentate and two unidentate nitrates. From these results, it is proposed that in media containing a large excess of NO_3^- the $[UO_2(NO_3)_4]^{2-}$ species is formed.

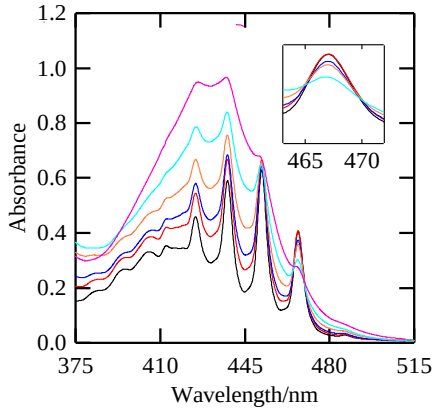

Fig. 1. Changes in UV-vis absorption spectra with the addition of [EMI][NO_3] (a: 0, b: 0.050, c: 0.10, d: 0.20, e: 0.50, f: 1.5 M) to CH_3CN dissolved $[EMI]_2[UO_2(NO_3)_4]$ (24 mM). Temp. = 50 °C.

REFERENCES:

[1] L.K. Kaplan, R.A. Hildebrandt, and M. Ader, *J. Inorg. Nucl., Chem.*, **2** (1956) 153.
[2] J.L. Ryan, *J. Phys. Chem.*, **65** (1961) 1099.
[3] R.D. Denning, D.N.P. Foster, T.R. Snellgrove, and D.R. Woodwark, *Mol. Phys.*, **37** (1979) 1089.
[4] K. Servaes, C. Hennig, I. Billard, C. Gaillard, K. Binnemans, C.G-.Walrand, and R.V. Deun, *Eur. J. Inorg. Chem.*, (2007) 5120.
[5] P. Nockemann, K. Servaes, R.V. Deun, K.V. Hecje, L.V. Meervelt, K. Binnemans, and C.G-Walrand, *Inorg. Chem.*, **46** (2007) 11335.
[6] D.L. Quach, C.M. Wai, and S.P. Pasilis, *Inorg. Chem.*, **49** (2010) 8568.
[7] S. Georg, I. Billard, A. Ouadi, C. Gillard, L. Petitjean, M. Picquet, and V. Solo'ev, *J. Phys. Chem. B*, **114** (2010) 4276.
[8] A.E. Bradley, C. Hardacre, M. Nieiwenhuyzen, W.P. Pitner, D. Sanders, K.R. Seddon, and R.C. Thied, *Inorg. Chem.*, **43** (2004) 2503.
[9] C. Gaillard, O. Klimchuk, A. Ouadi, I. Bikkard, and C. Hennig., *Dalton Trans.*, **41** (2012) 5476.

採択課題番号 25P1-5　　f-元素の有効利用に関わる基礎及び応用研究　　プロジェクト
（東工大・原子炉）佐々木琴江、鈴木智也、原田雅幸、池田泰久

PR1-6 Chemical Isotope Effect of Actinides and Fission Product Elements

T. Fujii, S. Fukutani and H. Yamana,

Research Reactor Institute, Kyoto University

INTRODUCTION: Isotope fractionation is originated from isotopic differences in nuclear mass, volume, and spin [1]. The equilibrium constant of the isotope exchange reaction can be theoretically obtained as the reduced partition function ratio (RPFR) of isotopologues [2]. The RPFR value due to the vibrational isotope effect is calculated through vibrational frequency analysis. In this study, we report some experimental and theoretical results of intramolecular vibrations of uranyl UO_2^{2+} species.

EXPERIMENTAL: Weighed amounts of chloride salt and H_2O were mixed for preparing highly concentrated chloride solutions of alkali chlorides and alkakine earth chlorides. A portion of the starting material (HCl containing U(VI)) was once dried by heating and then the chloride matrix solution prepared was added. The concentration of U was 0.01 mol dm^{-3} (M). Electronic absorption spectra of the samples were measured by using an UV/Vis/NIR spectrophotometer (Shimadzu, UV-3100PC).

COMPUTATIONAL DATAILS: The orbital geometries and vibrational frequencies of aqueous U(VI) species were calculated by using the density functional theory (DFT) as implemented by the Gaussian09 code [3]. The DFT method employed here is a hybrid density functional consisting of Becke's three-parameter non-local hybrid exchange potential (B3) with Lee-Yang-and Parr (LYP) non-local functionals. The 6-31G(d) basis set was chosen for H, O, and Cl, and the Stuttgart/Dresden basis set (SDD) for U.

RESULTS: Absorption spectra of chloride samples including UO_2^{2+} species are shown in Fig. 1. Specific absorption bands can be seen in the wavelength range of 350-500 nm. For each system, several absorption peaks due to intramolecular vibrations of UO_2^{2+} species were found. The vibrational frequency of totally symmetric vibrational mode (ν_1) has been reported to be 872 cm^{-1} for hydrated UO_2^{2+} [4]. Hydrated uranyl ion of U(VI) in aqueous solutions is known to be $UO_2(H_2O)_5^{2+}$, and water molecules at the equatorial plane are substituted by Cl^- ions in concentrated chloride systems [5].

Orbital geometries and vibrational frequencies of uranyl species were computed by using DFT. The vibrational frequency calculated for uranyl species are shown in Fig. 2. Use of a small cluster model with B3LYP resulted in overestimation of the ν_1 frequency. The ν_1 frequencies were found to be in the order of UO_2^{2+} > UO_2Cl^+ > $UO_2Cl_2^0$. This is consistent with the literature [6]. Ligand exchange of water molecules by Cl^- ions at the equatorial plane of UO_2^{2+} in concentrated chloride solutions decreases its ν_1 frequency.

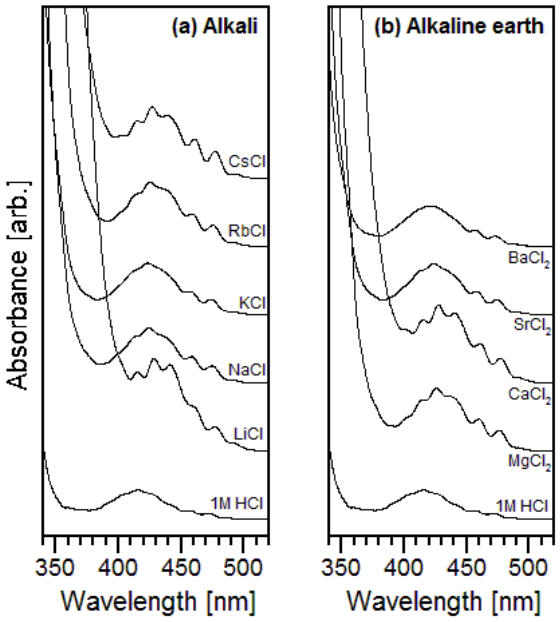

Fig. 1. Absorption spectra of chloride systems including 0.01 M U(VI).

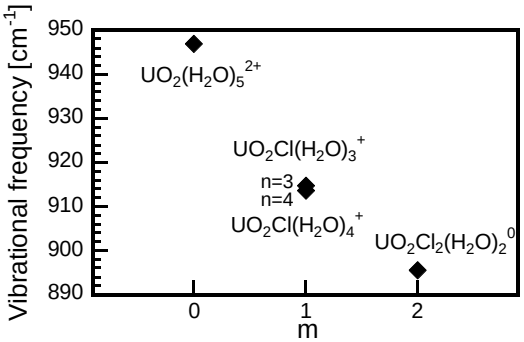

Fig. 2. ν_1 frequency computed for $UO_2Cl_m(H_2O)_n^{2-m}$.

REFERENCES:

[1] T. Fujii *et al*., Chem. Geol. **267** (2009) 139.
[2] J. Bigeleisen and M. G. Mayer, J. Chem. Phys. **15** (1947) 261.
[3] M. J. Frisch *et al*., Gaussian 09, Revision B.01 Gaussian Inc. (2009).
[4] T. Fujii *et al*., J. Alloys Compd. 323-324 (2001) 859.
[5] A. Uehara *et al*., NEA/NSC/DOC **15** (2009) 197.
[6] C Nguyen-Trung *et al*., Inorg Chem **31** (1992) 5280.

採択課題番号 25P1-6　アクチニド元素及び FP 元素の化学同位体効果に関する研究　プロジェクト
（京大・原子炉）藤井俊行、福谷　哲、山名　元

PR1-7

Isotope Separation by Microreactor

R. Hazama, Y. Sakuma[1], A. Ito, T. Fujii[2], T. Fukutani[2] and Y. Shibahara[2]

Graduate School of Human Environment, Osaka Sangyo University
[1]Research Laboratory for Nuclear Reactors, Tokyo Institute of Technology,
[2]Research Reactor Institute, Kyoto University

INTRODUCTION: The application of recent advances in microchip technology to our liquid-gas extraction by utilizing circulated liquid-gas multi phase flow in a microchannel chip without any stirring will be quite attractive. Now the widest variety of stable isotopes is mainly separated at electromagnetic separators and gas centrifuges. Flexible highly efficient centrifugal technology is only possible for those elements (about 20) which have gaseous compounds at room temperature. Therefore, these methods cannot meet the separation of calcium isotopes. The neutrino-less double beta decay is acquiring great interest after the confirmation of neutrino oscillation which demonstrated nonzero neutrino mass. Measurement of neutrino-less double beta decay provides a test for the Majorana nature of neutrinos and gives an absolute scale of the effective neutrino mass. Among double beta decay nuclei, ^{48}Ca has an advantage of the highest Q-value (4.27 MeV). The only drawback of ^{48}Ca is a small natural abundance of 0.187 %. In order to do a measurement with sensitivity to the mass region indicated by neutrino oscillation measurements, we have to prepare several tons of calcium. Thus, we proposed CANDLES (Calcium fluoride for the study of Neutrinos and Dark matters by Low Energy Spectrometer) system [3]. Currently we constructed the detector system CANDLES III at the Kamioka underground laboratory (2700 m.w.e.), which consists of 96 CaF_2(pure) scintillators with total mass of 305 kg and liquid scintillator with total volume of 2 m^3. At first, we found that calcium isotopes were actually fluctuated by liquid-liquid extraction using dicyclohexano-18-crown-6 and the advantage of our chemical exchange method is verified not only for an ion separation, but also for an isotope separation. We also evaluated each contribution ratio of the field shift effect and the hyperfine splitting shift effect to the mass effect of the calcium isotopes and found the contribution of the field shift effect is small [1]. Recently chromatography experiments using benzo-18-crown-6 resin were also carried out and calcium ion selectivity and isotope effects was observed [2]. However, it was found that the absorption of calcium depends on the concentration of "additional" hydrochloric acid in solution and its observed separation factor is about one order smaller than the direct liquid-liquid extraction. These indications are promising towards the calcium separation by the liquid-liquid phase transfer system with the help of a microchannel chemistry.

EXPERIMENTS: Isotopic enrichment occurs according to the following chemical exchange reaction:

$$^{40}Ca^{2+}_{(aq)} + {}^{48}CaL^{2+}_{(org)} \rightarrow {}^{48}Ca^{2+}_{(aq)} + {}^{40}CaL^{2+}_{(org)} \quad (1)$$

where L represents macrocyclic polyether(18-crown-6). As a result, ^{40}Ca is enriched in the organic-phase (org) crown solution and the heavy isotopes of ^{48}Ca tend to concentrate in the aqueous (aq) phase. The fractionation of ^{48}Ca from the most abundant isotope ^{40}Ca (96.9%) is the key to realize the chemical separation method by liquid-liquid extraction using a crown ether. Unfortunately the most abundant ^{40}Ca cannot be measured even by high resolution double-focusing sector field ICPMS, because the coincidence of $^{40}Ar^+$ and ^{40}Ca is the most annoying example of an isobaric interference and its required resolution (192498) is beyond ICP-MS's maximum resolution. Thus, we developed a new "multicollector technique" for the thermal ionization mass spectrometer (TIMS) measurement of calcium isotope ratios for the mass range from 40-48 atomic mass unit (amu). Before the TIMS measurement, residual organic substances and chlorine were removed by using ion-exchange resin (Dowex 50WX8) , the resultant Ca solutions were evaporated to dryness in PTFE teflon vials, and dissolved to 300 ppm (300 ng Ca/ μ L) solutions with HNO_3. It is noted that we used calcium carbonate powders (NIST SRM915b) as a Ca standard for the comparison with our samples and its feed solution for normalization procedures. It is noted that we succeeded to measure each Ca isotope as an accuracy of about 1 % and its isotopic ratio of ^{48}Ca/^{40}Ca with about 0.1 % for Ca standard solution.

REFERENCES:

[1] R. Hazama *et al.*, Proc. of 6th Rencontres du Vietnam, Gioi Publishers (2007) 383: arXiv0710.3840.[nucl-ex].
[2] K. Hayasaka, T. Kaneshiki, M. Nomura, T. Suzuki, Y. Fujii, Prog. Nucl. Ener. **50** (2008) 510.

採択課題番号 25P1-7　　マイクロリアクターによる同位体分離　　プロジェクト
（大産大院・人間環境）硲　隆太、伊藤彩　（東工大・原子炉研）佐久間洋一
（京大・原子炉）藤井俊行、福谷哲、芝原雄司

PR1-8 Sr Isotopic Compositions of Double Spike Enriched with ^{84}Sr and ^{87}Sr

T. Shibata, M. Yoshikawa, T. Fujii[1], S. Fukutani[1] and Y. Shibahara[1]

Institute for Geothermal Sciences, Kyoto University
[1]Research Reactor Institute, Kyoto University

INTRODUCTION: The isotopic composition of Sr has been used for a useful geochemical tool to discuss the genesis and ages of terrestrial and exterritorial materials. Sr has five, naturally occurring isotopes, those are ^{84}Sr, ^{86}Sr, ^{87}Sr and ^{88}Sr. Only ^{87}Sr is radiogenic, and the others are stable isotope, respectively. Traditionally, ratios among stable isotopes have been considered to be constant values in order to correct instrumental mass fractionation during measurement of the radiogenic strontium ratio ($^{87}Sr/^{86}Sr$). Recently, however, variations of $^{88}Sr/^{86}Sr$ are observed from sea water, river water and carbonates from the results of inductively coupled plasma mass spectrometry (MS) [1], and analytical methods employed by thermal ionization MS (TIMS) with double spike are developing to measure more precise $^{88}Sr/^{86}Sr$ ratios [1,2]. The double spike method can also be applied to the measurements for short-lived isotopes, such as ^{90}Sr. We, therefore, tried to establish the Sr double spike method, and report the isotopic compositions of Sr double spike and $^{88}Sr/^{86}Sr$ ratios of NIST SRM987.

Experiments: Samples to be analyzed are prepared as follows; NIST SRM987 is diluted with nitric acid to be obtained 100 ppm solution and the ^{84}Sr and ^{87}enriched spikes are mixed to be the $^{87}Sr/^{84}Sr$ ratio is closed to the unity. Each solution is loaded onto Re-filament. Solutions of NIST SRM987 and double spike are mixed on the Re-filament. The loaded samples of double spike (n = 2), NIST SRM987 (n = 6) and mixed sample (n = 1) are measured to obtain $^{86}Sr/^{84}Sr$, $^{87}Sr/^{84}Sr$, $^{88}Sr/^{84}Sr$ and $^{88}Sr/^{86}Sr$ ratios. The TIMS of Triton TL at Research Reactor Institute, Kyoto University is used for the measurements. The $^{87}Sr/^{86}Sr$ ratios of NIST SRM987, which are corrected the instrumental mass fractionation using a factor of $^{88}Sr/^{86}Sr = 0.1194$, show the reproducibility of 0.7102448 ± 0.0000067 (1σ, n = 6). The isotopic compositions of Sr double spike and $^{88}Sr/^{86}Sr$ ratios of NIST SRM987 are calculated using by the visual basic and solver analyses of Microsoft Excel following the algorism shown by [3].

RESULTS: The Sr isotopic compositions of double spike are estimated as follows; 1) calculate $^{88}Sr/^{86}Sr$ ratios of NIST SRM987 from the measured ratios of NIST SRM987 and mixed samples with those of double spike, 2) changing the factor of instrumental mass fractionation during measurement for double spike, and find a fractionation factor, which makes a deviation of calculated $^{88}Sr/^{86}Sr$ ratios of NIST SRM987 from recommended one to be minimum and 3) Sr isotopic compositions of double spike are calculate using by the fractionation factor determined by 2). The estimated Sr isotopic compositions of double spike are shown in Table 1. The $^{88}Sr/^{86}Sr$ ratios and $\delta^{88/86}Sr$ of NIST SRM987 analyzed by the double spike method is shown in Table2 and Fig. 1.

	$^{88}Sr/^{86}Sr$	$^{87}Sr/^{84}Sr$	$^{86}Sr/^{84}Sr$
Double Spike	0.118831	0.95331	0.016446

Table 1. Sr isotopic compositions of the double spike..

	$^{88}Sr/^{86}Sr$	$\delta^{88/86}Sr$
NIST 987	8.37552	0.037
	8.37526	0.006
	8.37529	0.009
	8.37483	-0.046
	8.37495	-0.031
	8.37541	0.024

Table 2. $^{88}Sr/^{86}Sr$ ratios and $\delta^{88/86}Sr$ of NIST SRM987 analyzed by the double spike method. $\delta^{88/86}Sr$ is the deviation from recommended value of $^{88}Sr/^{86}Sr$ ratio (8.375209) of NIST SRM987, expressed with part per thousand (‰).

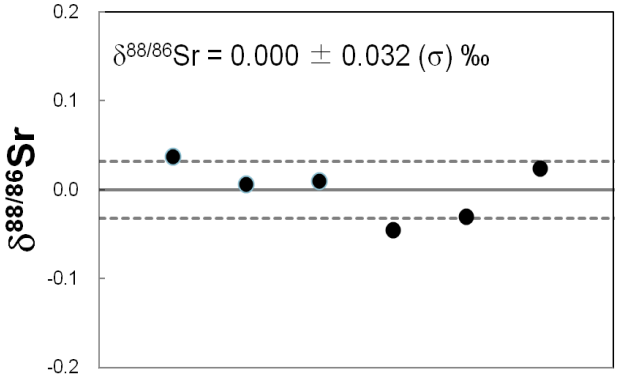

Fig. 1. $\delta^{88/86}Sr$ of NIST SRM987 analyzed by the double spike method.

REFERENCES:

[1] Cavazzini, G., Int. J. Mass Spec., **240** (2005) 17–26.
[2] J. Fietzke, J. and A. Eisenhauer, G3, 7, doi: 10.1029/2006GC001243 (2006)
[3] A. Krabbenhöft *et al*., J. Anal. At. Spectrom, **24** (2009) 1267 – 1271.

採択課題番号 25P1-8　　火山地帯の地下水・熱水と岩石間の　　プロジェクト
ランタニド・アクチノイド含む微量元素濃度の測定方の開発
（京大・理）柴田知之、藤井俊行、福谷　哲

PR1-9 Redox Behavior of Uranium at Silicon Electrode in LiCl-KCl Eutectic Melt

Y. Sakamura, T. Murakami, M. Iizuka, K. Uozumi,
T. Fujii[1], A. Uehara[1] and H. Yamana[1]

Central Research Institute of Electric Power Industry
[1]Research Reactor Institute, Kyoto University

INTRODUCTION: Electrorefining process using a molten chloride salt bath has been developed for treating spent nuclear fuels in the chemical forms of metal, nitride and oxide. Uranium silicide fuels are used for research reactors. The U-Si binary phase diagram and thermodynamic properties of the U-Si compounds have been reported [1, 2]. However, electrochemical behaviors of the U-Si compounds in molten chloride systems have not yet been investigated. In this study, redox behavior of uranium at a silicon electrode was examined by cyclic voltammetry in a LiCl-KCl eutectic melt containing UCl_3.

EXPERIMENTS: A LiCl-KCl eutectic melt with dissolved UCl_3 (0.23 mol%) was contained by an alumina crucible at 773 K. The Ag/AgCl reference electrode consisted of a silver wire immersed in a LiCl-KCl eutectic salt mixture with 1 wt% AgCl, which was contained in a closed-end Pyrex tube. A glassy carbon rod (3 mm diameter) was used as the counter electrode. A tungsten wire (1 mm diameter) and a silicon chip (99.9999% purity) shown in Fig. 1 were used as the working electrode. The tungsten metal was employed as the inert electrode because it does not form any alloys with uranium or lithium metal. All the measurements were conducted in a high-purity Ar atmosphere glove box (H_2O, O_2 < 2 ppm).

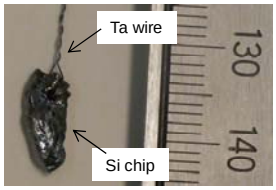

Fig. 1 Si electrode with Ta wire lead

RESULTS: The blank test was conducted in a LiCl-KCl eutectic alone. The potentials of Li/Li^+ and Cl^-/Cl_2 in this system were -2.4 and +1.2 V, respectively. The cyclic voltammetry was conducted using the Si electrode of which front edge was immersed in the melt. As shown in Fig. 2, the cyclic voltammogram (CV) has a cathodic current rising at about -2.1 V, which might correspond to the formation of Li-Si compound. The anodic current rising at about 0.8 V might be due to the evolution of silicon chloride gas.

Figure 3 shows typical CVs of W and Si electrodes in the LiCl-KCl-UCl_3 melt. The CV of W is similar to those previously reported [3]. The reduction of U^{3+} to U metal occurred by a one-step process for the reduction wave rising at -1.4 V, followed by reoxidation of the deposited U metal at the electrode surface during the anodic sweep. The anodic peak at -0.10 V corresponds to the oxidation of U^{3+} to U^{4+}.The small cathodic peak at -1.3 V and the anodic peak at -0.6 V might be due to the adsorption and desorption of U on the W electrode, respectively.

On the Si electrode, a cathodic current rises from -0.9 V. It is much more positive than the U deposition potential on the W electrode, indicating that stable U-Si compounds formed at the electrode surface. Several compounds (USi_3, USi_2, U_2Si_3, USi, U_3Si_2 and U_3Si) are shown in the U-Si phase diagram [1]. There are a couple of anodic waves corresponding to the U dissolution from the different U-Si compounds. It is suggested that the U might dissolve from the U-Si compounds with high Si/U ratio along with the oxidation of U^{3+} to U^{4+}, which should cause the low current efficiency for the electrorefining of spent silicide fuels. Identification of the U-Si compounds is the next subject of this study.

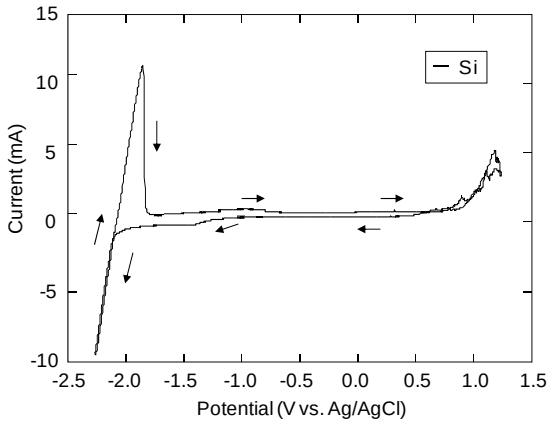

Fig. 2 CV of Si electrode in LiCl-KCl eutectic melt at 773 K. Scan rate 0.1 V/s.

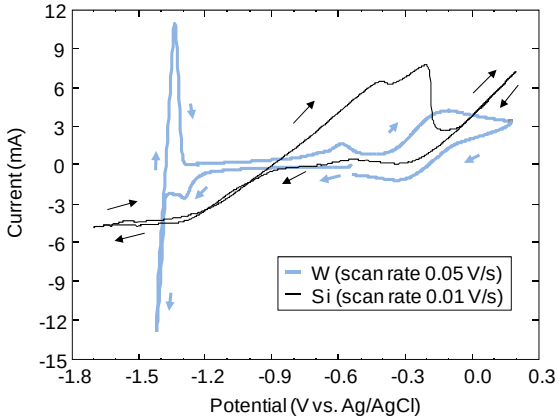

Fig. 3 CVs of W and Si electrodes in LiCl-KCl eutectic melt containing 0.23 mol% of UCl_3 at 773 K.

REFERENCES:

[1] T.B. Massalski, *Binary Alloy Phase Diagrams*, Vol. 1, American Society for Metals, Metals Park, OH, 1986.
[2] A. Berche *et al.*, J. Nucl. Mater., **389** (2009) 101-107.
[3] P. Masset *et al.*, J. Electrochem. Soc., **152** (2005) A1109-A1115.

採択課題番号 P1−9 乾式再処理系でのウランの電気化学研究 プロジェクト
(電中研)坂村義治、村上 毅、飯塚政利、魚住浩一 (京大・原子炉) 山名 元、藤井俊之、上原章寛

PR1-10 Effect of Fluoride Addition on UV-vis Spectra of Neodymium Cation in Molten NaCl-2CsCl

H. Matsuura, A. Nezu, H. Akatsuka, A. Uehara[1], H. Yamana[1] and T. Fujii[1]

Research Laboratory for Nuclear Reactors, Tokyo Institute of Technology
[1]Research Reactor Institute, Kyoto University

INTRODUCTION: Neodymium is the one of the rare earth fission products and was utilized as the prototype of some trans uranium elements due to its similarity of electrochemical behavior. Also, neodymium is one of important materials since it has been widely utilized at magnets in the motors, and effective recycling technology from the end produncts has been waiting for a long time. Although molten salt should be relatively constructed by a simple structural model due to the predominant ionic species in liquid phase, several electrochemical behaviors have not been well understood by the microscopic point of view. For a recent few years, the electrochemical behavior of rare earths including neodymium in the molten chlorides with small amount of fluorides has been focused, and structural elucidation by extended absorption fine structure and UV-vis spectroscopy of neodymium in molten salts has been performed. In this year, fluoride concentration dependence on the spectra of neodymium in molten NaCl-2CsCl-$NdCl_3$-NaF was measured more precisely than previous year and the structural variation is discussed by some parameters derived from the Judd-Ofelt analysis.

EXPERIMENTS: UV-vis spectroscopy of neodymium in molten NaCl-2CsCl-$NdCl_3$-NaF at 953 K has been carried out by using the spectrophotometer (JASCO V-500) in KURRI[1]. A quartz cell with 10mm of light path was used for the molten salt container, and experimental procedure was exactly the same as that described in the report of the last year. For the calculation of oscillator strength of the hypersensitive transition and derivation of $\Omega_{2,4,6}$ parameters by the Judd-Ofelt analysis, density was assumed to be the additivity of molar volume of each component, and refractive index was temporary used from the value of KCl due to the non-availability of the data of CsCl.

RESULTS and DISCUSSION: Figure 1 shows the variation of oscillator strength of hypersensitive transition absorption of neodymium at ca. 589 nm depending on fluoride addition. This peak has been considered to the indication of coordination symmetry around neodymium cation, i.e. 6 coordinated octahedral species, and the smaller value relates to more perfectly symmetric (more stabilized) structure [2]. One striking feature of this figure is that with increasing fluoride amount until ca. F/Nd = 2, the value of oscillator strength increases and decreases over F/Nd = 2, and decreases rapidly over ca. F/Nd = 5. This means that octahedral chloride coordinated structure is once un-stabilized by the addition of fluoride and stabilized by adding further, which would well relate to anomalous variation of electroreduction potential depending on fluoride concentration [3].

Figure 2 shows $\Omega_{2,4,6}$ values derived by the Judd-Ofelt analysis. Ω_2 value is in the trend of decreasing with increasing F/Nd ratio, but at ca. F/Nd = 3, small hump appears. Smaller value of Ω_2 is considered to relate corvalency of local structure around neodymium cation, thus the melt around F/Nd = 3 may take un-stabilized structure, in which local coordinated chlorides are half exchanged by fluorides. Ω_4, which is suggested to relate the mixing effect of electrons from coordinated species, seems to show much complicated tendency depending on F/Nd ratio, thus further systematic investigation on the similar mixture systems would be required.

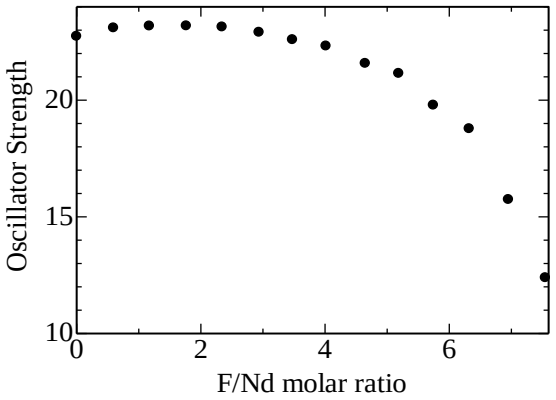

Fig. 1 Oscillator strengths of the electronic absorption spectra of neodymium in molten NaCl-2CsCl-NaF.

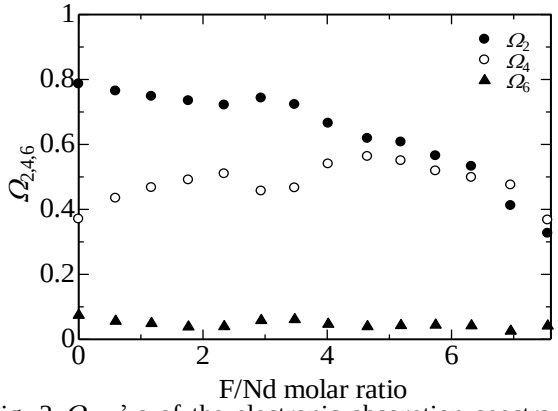

Fig. 2 $\Omega_{2,4,6}$' s of the electronic absorption spectra of neodymium in molten NaCl-2CsCl-NaF.

REFERENCES:

[1] T. Fujii *et al.*, J. Alloys Compd., **393** (2005) L1.
[2] Yu. A. Barbanel *et al*, J. Radioanal. Nucl. Chem., **143** (1990) 167.
[3] K. Fujita, Master thesis, Tokyo Tech. (2013).

採択課題番号 25P1-10　アクチニド元素及び FP 元素含有ハロゲン化物の XAFS 構造解析および可視紫外分光研究　プロジェクト
（東工大・原子炉研）松浦治明、根津　篤、赤塚　洋
（京大・原子炉）上原章寛、山名　元、藤井俊行

PR1-11 Electrochemical and Spectrophotometric Measurement of Zirconium Ion in High Temperature Molten LiCl-KCl Eutectic

A. Uehara, T. Nagai[1], T. Fujii and H. Yamana

Research Reactor Institute, Kyoto University
[1]Nuclear Fuel Cycle Engineering Lab., Japan Atomic Energy Agency

INTRODUCTION:

Pyroelectrochemical processes based on molten chloride electrolyte system have over the past decade received substantial interest for the reprocessing of irradiated nuclear fuel. Since zirconium is a major component in reactor fuel types such as Uranium-zirconium, in a pyro-electrometallugical reprocessing context, it is reasonable to expect that a proportion of zirconium could be carried over into a molten salt electrolyte and as such could interfere with the recovery of actinides [1]. In the present study, the reaction mechanism of zirconium reduction in molten LiCl-KCl eutectic was investigated using electrochemical and spectrophotometric method.

EXPERIMENTAL:

For the cyclic voltammetry experiment of LiCl-KCl eutectic system, about 0.1 mol% $ZrCl_4$ solutions of molten LiCl-KCl (59 : 41) eutectic was used. Quartz tubes of 13 mm inner diameter were used for the measurement. A 1.0 mmϕ tungsten rod was used for working electrode and a pyro-graphite carbon rod of 3 mmϕ was used for the counter electrode. An $Ag|Ag^+$ reference electrode composed with an Ag wire|1 mol% AgCl in a bulk melt|PYREX glass membrane tube was used. Electrochemical measurement system HZ-5000 (Hokuto-Denko Co. Ltd.) was used for the voltammetry measurements. The constant potential electrolysis was performed using Ag wire and LiCl-KCl contained in a PYREX glass membrane tube as counter electrode to avoid cyclic redox reaction between tungsten working and counter electrode. After sufficient hours of electrolysis for completing the reduction, sample solution was taken by sampling glass tube. All the experiments were carried out in a glove box filled with dry argon whose humidity and oxygen impurity was continuously kept less than 1 ppm.

RESULTS:

Cyclic voltammogram was measured in molten LiCl-KCl eutectic containing 0.44 mol% $ZrCl_4$ at 773K. two cathodic current peaks and three anodic currents peaks were observed, these current increase with increase of potential scanning rate. Zr(IV) was reduced to Zr(II) when cathode potential is more negative than −0.8 V (vs. 1 mol% Ag/AgCl) as Eq.(1);

$$Zr(IV) + 2e^- \rightarrow Zr(II) \quad (1)$$

Zr(II) was reduced into Zr metal when cathode potential was more negative than −1.0 V as Eq.(2);.

$$Zr(II) + 2e^- \rightarrow Zr \quad (2)$$

On the other hand, Park et al [2] reported that ZrCl was formed at -1.0V which is insoluble or metastable in the melt. In order to confirm the reaction, bulk electrolysis was carried out by applying -0.85 V. Black deposit was shown at the inner surface of the cell. Though XRD analysis was carried out, the ZrCl was not confirmed because of the oxidation but ZrO_2 (Fig. 3).

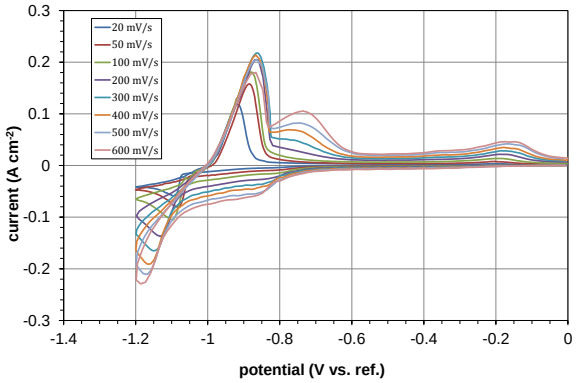

Fig. 1. Cyclic voltammogram for the redox of Zr ions measured in molten LiCl-KCl eutectic at 773K.

Fig. 2. Deposit formed at the surface of the quartz cell after the electrolysis applied at -1 V for 13 hours.

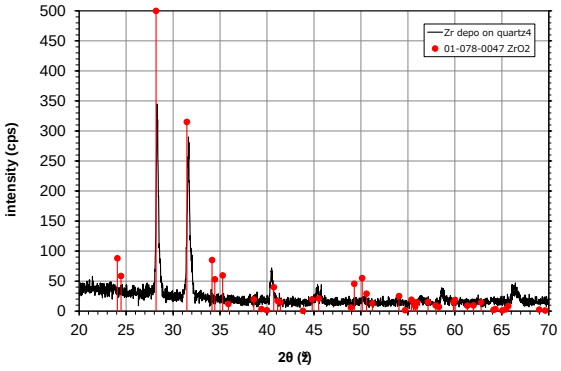

Fig. 3. XRD data measured at the surface of quartz cell.

REFERENCES:

[1] CP. Fabian, et al., J. Electrochem. Soc., **160** (2013) H81-86.
[2] J. Park, et al., J. Electrochem. Soc., **161** (2014) H97-104.

採択課題番号 25P1-11　溶融塩及び水和物溶融体中におけるアクチノイドイオンの分光電気化学的研究　プロジェクト

（京大・原子炉）上原章寛、藤井俊行、森山裕丈、山名　元（原子力機構）永井崇之

PR1-12 Structural Analysis of Uranyl Ion in 14M LiCl Aqueous Solution

N. Ohtori, Y. Ishii, A. Uehara[1], T. Fujii[1], H. Yamana[1] and Y. Okamoto[2].

Department of Chemistry, Niigata University
[1]Research Reactor Institute, Kyoto University
[2]Japan Atomic Energy Agency

INTRODUCTION: Hydrate melts such as concentrated alkali halide aqueous solutions attract some recent attention as a novel candidate for solvents useful for reprocessing of spent nuclear fuels[1]. We performed molecular dynamics (MD) simulation of LiCl aqueous solutions containing uranyl ion and reported some results such as diffusion coefficients and average local structure around uranyl ion in the previous report[2]. In this work, we have analyzed coordination structure around uranyl ions in 14 M LiCl aqueous solution in more detail and compared the results with experimental results[3].

CALCULATIONS: MD calculation has been performed under *NVE* ensemble. The SPC/E model was used for water molecule. The other parameters were cited from ref [4,5]. The water and uranyl molecules were constrained by SHAKE algorithm. A simulation cell contained 2 uranyl chloride ion pairs, 560 LiCl ion pairs, and 1563 water molecules, corresponding 14M LiCl aqueous solution. Time step was 1.0 fs. After the equilibration at 298K for 10 ps, coordination structure of uranyl ion was evaluated in detail. We calculated the U L_{III}-edge EXAFS spectrum by using the FEFF code[6], comparing with the experimental result [3].

RESULTS: Table 1 shows coordination number distribution for uranyl ion. In our MD simulation of 14 M LiCl aqueous solution, each uranyl ion had 5-coordinated structure, which consists of 3.98 water and 1.02 chloride ion as their average values. As the coordination structure around uranyl ion are shown in Fig.1, these water molecules and chloride ions are located on the equatorial plane. Figure 2 shows EXAFS spectra evaluated using each coordination structure indicated in Table 1. All the spectra of coordination structures don't fit very well to the experimental result[3], which suggests that there is some room to modify the interaction potential model of uranyl ion in 14 M LiCl aqueous solutions.

Table 1 Coordination numbers distribution for uranyl ion in 14 M LiCl aqueous solution.

Coordination ligand		Abundance / %
water	Cl^-	
5	0	15.4
4	1	66.0
3	2	17.8

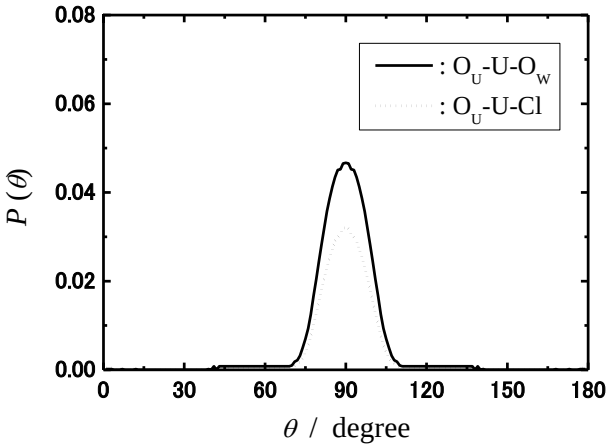

Fig.1 Angular distribution of the uranyl ion coordinated by water or chloride ion in 14 M LiCl aqueous solution.

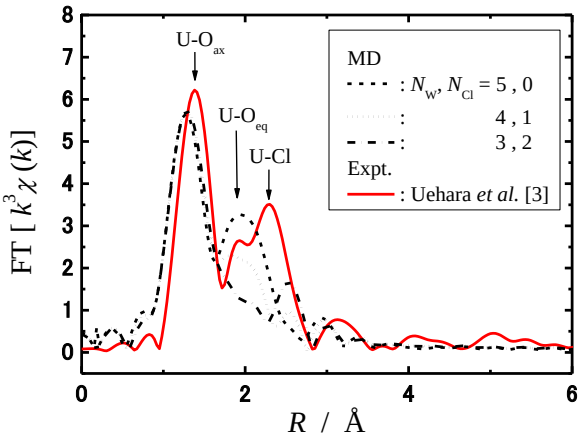

Fig.2 Fourier transforms of experimental and calculated U L_{III}-edge EXAFS spectra in 14 M LiCl aqueous solution.

REFERENCES:

[1] A. Uehara, O. Shirai, T. Fujii, T. Nagai and H. Yamana, *J. Appl. Electrochem.*, **42** (2012)455.
[2] N. Ohtori, Y. Ishii, A. Uehara, T. Fujii, H. Yamana, K. Minato and Y. Okamoto, KURRI Progress Report, PR2-1(2013).
[3] A. Uehara, T. Fujii, H. Matsuura, N. Sato, H. Yamana and Y. Okamoto, *OECD-NEA*, **15** (2009) 197.
[4] P. Guilbaud and G. Wipff, J. Mol. Struct., **366** (1996) 55.
[5] S. H. Lee and J. C. Rasaiah, *J. Phys. Chem.*, **100**, (1996) 1420.
[6] A. L. Aukudinov, B. Ravel, J. J. Rehr and S. D. Conradson, *Phys. Rev. B*, **58** (1998) 7565.

採択課題番号 25P1-12　融体中での f-元素の分子動力学計算と実験系の照合研究　プロジェクト
（新潟大・理）大鳥範和、石井良樹　（京大・原子炉）上原章寛、藤井俊行、山名　元
（JAEA）岡本芳浩

PR1-13

Experimental and Calculated Optical Properties of Molten Alumnium Chloride Melts

T. Goto, K. Hachya[1], A. Uehara[2], T. Fujii[2] and H. Yamana[2]

Graduate School of Science and Engineering, Doshisha University
[1]Graduate School of Energy Science, Kyoto University
[2] Research Reactor Institute, Kyoto University

INTRODUCTION: Molten $AlCl_3$ and *A*Cl-$AlCl_3$ (*A*: alkaline metals) have been attractive targets of studies from both fundamental and application viewpoints, because of their relatively low melting points which lead to their effectiveness. The structure of the melts contains a variety of coordinations which have long been investigated and mainly consists of covalent bonding between Al-Cl. In this study, Raman scattering measurements are performed to investigate into their bonding structures, and the spectra are analyzed with *ab initio* simulations. We focus our study on CsCl-$AlCl_3$ binary and LiCl-KCl-CsCl-$AlCl_3$ quaternary systems.

EXPERIMENTS: JASCO NRS-3100 Raman spectrometer in KURRI was used to obtain Raman scattering spectra for $AlCl_3$, LiCl-KCl eutectic melt - $AlCl_3$ (3 mol%), LiCl-KCl-CsCl eutectic melt - $AlCl_3$ (3 mol%), and NaCl-$AlCl_3$ 1:1 melt. The simulated spectra and up to 2 ps trajectories of ions in the melts were calculated with GAUSSIAN09 simulation package.

RESULTS: The obtained Raman scattering spectra for molten $AlCl_3$ and simulated spectra are given in Fig. 1, using B3LYP calculations in GAUSSIAN09. Characteristic scattering bands are reproduced in the calculated spectra, and attributed to appropriate vibration modes. A variant of first-principle molecular dynamics simulations, ADMP (Atom-centered Density Matrix Propagation) calculation of the ionic trajectories were performed for CsCl-$AlCl_3$ at 700 K. As comprehensively reviewed in Ref. [1], up to 1 : 1 mixture of CsCl/$AlCl_3$ is expected to exclusively contain $AlCl_4^-$ cluster as an anion. We can also observe $Al_2Cl_7^-$ at least as an temporary structure in Fig. 2. In addition, $AlCl_4^-$ clusters are not always rigid, and Cl^- ions are exchanged among clusters as can be seen in Fig. 3.

DISCUSSIONS: In aluminum chloride melts, six-fold Cl-atom coordination around an Al atom is changed to four-fold coordination to form $AlCl_4^-$ anion, and it is stable to maintain the cluster structure even when mixed with alkaline chlorides. Nevertheless, connection between $AlCl_4^-$ tetrahedra has certain variety. For example, in pure $AlCl_3$ melt, edge-sharing two tetrahedra, Al_2Cl_6 structure has a dominance. For CsCl-$AlCl_3$ mixture system, on the other hands, anion structure of isolate $AlCl_4^-$ tetrahedra shift to corner-sharing two-tetrahedron structure, $Al_2Cl_7^-$, dramatically at 1 : 1-ratio with increasing CsCl content. Our calculation seems to reproduce fluctuations in the structural rearrangement at that mixing ratio.

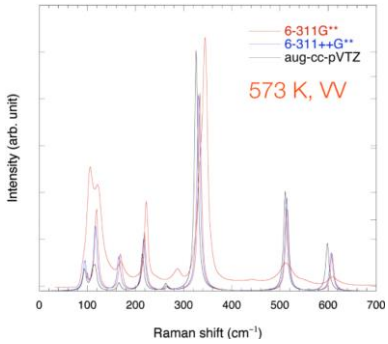

Fig. 1 Experimental Raman spectra for molten $AlCl_3$ at 573 K and simulated spectra for Al_2Cl_6 clusters.

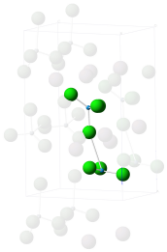

Fig. 2 Schematic of the structure in ADMP simulation at 0.35 ps. $Al_2Cl_7^-$-like clusters are highlighted.

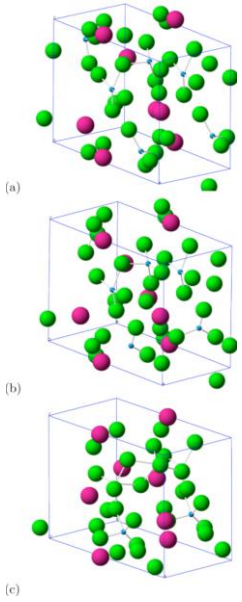

Fig. 3 Snapshot of the structure in ADMP simulation at (a) 1.25, (b) 1.5 and (c) 2 ps.

REFERENCE:

[1] M. P. Tosi, D. L. Price, M.-L. Saboungi, *Annu. Rev. Phys. Chem.*, **44** (1993) 173.

採択課題番号 25P1-13　　f－元素の有効利用に関わる基礎及び応用研究　　プロジェクト
（同志社大・理工）後藤琢也（京大院・エネ科）蜂谷　寛
（京大・原子炉）上原章寛、藤井俊行、山名　元

PR1-14

Electrochemical Behavior of Neodymium in $CaCl_2$ Based Molten Salt Containing Nd_2O_3-B_2O_3 Slag

H. Sekimoto, A. Uehara[1], T. Fujii[1] and H. Yamana[1]

Faculty of Engineering, Iwate University
Department of Materials Science and Engineering
[1]Graduate School of Science, Kyoto University[4]Research Reactor Institute, Kyoto University

INTRODUCTION: Development of recycling technique for neodymium magnet is essentially important to achieve sustainable society. Consequently, we propose and are investigating a new recycling process of neodymium magnet shown in Fig. 1. In the process, the neodymium magnet is melted together with sufficient amount of B_2O_3 in graphite crucible to form molten iron based alloy, B_2O_3 slag and Nd_2O_3-B_2O_3 slag, which is recovered and dissolved in molten salt. And then, Fe-Nd-B alloy is produced by electrolysis. In this study, electrochemical properties of neodymium and boron in $CaCl_2$ molten salt were investigated by cyclic voltammetry.

EXPERIMENTS: Experiments were conducted in an argon-filled glove box where both the oxygen content and the water content were controlled below 1 ppm. 3 gram of pure $CaCl_2$ was inserted in a cylindrical silica tube and melted at 800 °C. Cyclic voltammetry was then conducted. When potential was cathodically polarized, iron or tungsten rod was used for working electrode. When potential was anordically polarized, pyro-graphite rod was used. In both case, counter electrode was pyro-graphite rod and reference electrode was silver wire immersed in 1 mol%AgCl-$CaCl_2$ molten salt and electrochemically contacted in $CaCl_2$ molten salt via thin pyrex grass. After that, saturating amount of Nd_2O_3-B_2O_3 slag which is prepared by melting 5.7 gram of Nd_2O_3 and 4.3 gram of B_2O_3 in a graphite crucible at 1200 °C was added in the silica tube and held for 12 hours at 800 °C to obtain $CaCl_2$-Nd_2O_3-B_2O_3 molten salt. The concentration of Nd(III) in $CaCl_2$-Nd_2O_3-B_2O_3 molten salt is considered to be 0.114 mol kg^{-1}, which is the saturating concentration of Nd(III) [1]. Cyclic voltammetry was also conducted in the molten salt in the same manner. Based on the results of cyclic voltammetry, potential controlled electrolysis was conducted in $CaCl_2$-RE_xO_y-B_2O_3 molten salt which was prepared by similar manner to Nd_2O_3-B_2O_3 slag. Here, RE_xO_y-B_2O_3 slag was obtained by melting commercial neodymium permanent magnet together with sufficient amount of B_2O_3 in graphite crucible.

RESULTS: Figure 2 shows the cyclic voltammogram of $CaCl_2$ molten salt and $CaCl_2$-Nd_2O_3-B_2O_3 molten salt at 800 °C. In the case of $CaCl_2$ molten salt, cathodic current increased at -1.9 V vs Ag reference electrode in 1 mol%AgCl-$CaCl_2$ (AgCl/Ag), which is considered to correspond deposition of metallic calcium. Anordic current was increased at +1.1 V vs AgCl/Ag, which indicates that chlorine gas evolved at the potential. On the other hand, when potential was cathodically polarized in $CaCl_2$-Nd_2O_3-B_2O_3 molten salt, reduction current increased four times at -0.5, -0.6, -0.8, and -1.1 V vs AgCl/Ag. It is not possible to attribute these current increase to some reactions, but it is considered that they implies deposition of boron or formation of neodymium boride. The potential controlled electrolysis was conducted at -1.0 V vs AgCl/Ag using iron cathode and pyro-graphite anode. As the result, small amount of NdB_6 was obtained and the formation of NdOCl was observed in molten salt.

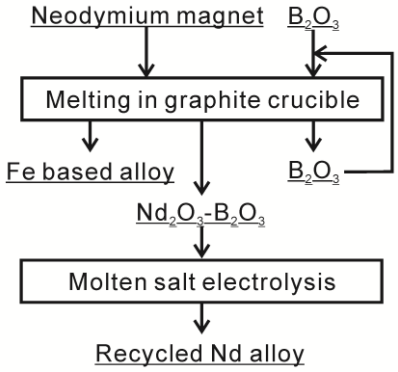

Fig. 1. Flowchart of the recycling process for neodymium magnet proposed in this study.

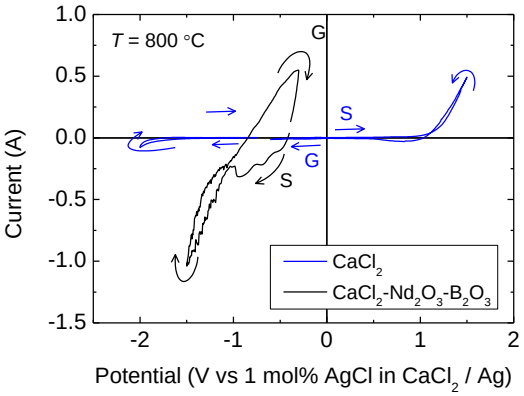

Fig. 2. Cyclic voltammogram of $CaCl_2$ molten salt and $CaCl_2$-Nd_2O_3-B_2O_3.

REFERENCES

[1] H. Sekimoto, A. Uehara, T. Fujii, H. Yamana, KURRI Progress report, (2012) 102.

採択課題番号 25P1-14　吸光分光測定を用いた高温融体中の金属イオンの溶存形態に関する研究　プロジェクト（f-元素の有効利用に関わる基礎及び応用研究）

（岩手大・工）関本　英弘
（京大・原子炉）上原　章寛、藤井　俊行、山名　元

PR1-15 Thermal Properties of Actinides-Containing Ceramics: Y_6UO_{12}

S. Yamanaka, Y. Ohishi, H. Muta and K. Kurosaki

Graduate School of Engineering, Osaka University

INTRODUCTION: The ceramic nuclear waste form has been considered as one of the methods to immobilize actinide elements extracted from high-level radioactive nuclear wastes. Among them, Y_6AnO_{12} where *An* represents actinide elements have received attention as appropriate ceramics in which actinide elements can be immobilized stably. When utilizing such ceramics as the waste form, the thermal properties such as thermal conductivity should be understood. However the properties of Y_6AnO_{12} have been scarcely reported. Our group has investigated the thermal properties of Y_6WO_{12} [1] because Y_6WO_{12} takes the same hexagonal crystal structure as that of Y_6AnO_{12} [2]. Here, polycrystalline samples of Y_6UO_{12} were synthesized by solid state reactions and the thermal conductivity was evaluated [3].

EXPERIMENT: Y_6UO_{12} was prepared from the mixtures of Y_2O_3 and U_3O_8 by standard solid-state reactions. Dried Y_2O_3 powders and U_3O_8 powders were weighed in the appropriate molar ratio and mixed, followed by pressing into pellets at 150 MPa for 5 min at room temperature. The green pellets were heated in air for 24 h at 1673 K. After that, in order to obtain high-density pellets, the spark plasma sintering (SPS) was conducted. The Y_6UO_{12} powders were put in a graphite die and heated up to 1573 K under the pressure of 50-80 MPa in an Ar-flow atmosphere. Since the oxygen loss might occur during the SPS due to the reduction by the graphite die, the oxygen supplementation was attempted. The pellets obtained by the SPS were heated in air for 48 h at 1673 K. Finally, the high-density (96% of the theoretical density) pellets were obtained. The samples were identified by XRD and SEM/EDX analyses. The thermal diffusivity (α) was measured by the laser flash method in vacuum from room temperature to 1173 K with the half-time method. The measurement was repeated three times at each temperature and the average value was taken as the measured valve. The specific heat capacity (C_P) of Y_6UO_{12} was estimated from Neumann Kopp's law using the data of Y_2O_3 and UO_3. The density (d) was calculated from the weight and the dimensions of the samples at room temperature. The thermal conductivity (κ) was evaluated according to the standard equation: $\kappa = \alpha C_P d$.

RESULTS: From the results of the XRD and SEM/EDX analyses, it was confirmed that the samples prepared in the present study were Y_6UO_{12} single phase materials with no impurity phases. Although a good single phase sample was obtained before SPS, the XRD pattern after SPS was changed most likely due to the oxygen loss during SPS. However, it was confirmed that a good single phase sample was obtained again after the heat treatment in air which was performed to supplement oxygen. The SEM and EDX mapping images indicated that the samples prepared in the present study were homogeneous with no secondary phases. It was also confirmed from the quantitative EDX analyses that the chemical composition did not deviate a lot from the starting composition. Temperature dependence of the κ of Y_6UO_{12} is shown in Fig. 2 [3], together with the data for Y_6WO_{12} and Yb_6WO_{12} previously obtained in our group [1]. The room temperature κ value of Y_6UO_{12} was 4.90 $Wm^{-1}K^{-1}$. The κ data shown in Fig. 1 were corrected to the data for 100% of the theoretical density by Schulz's equation [4]. The κ of Y_6UO_{12}, Y_6WO_{12}, and Yb_6WO_{12} decreased with increasing temperature in the whole temperature range, indicating that the phonon contribution to the thermal conduction was predominant. This is reasonable because Y_6UO_{12}, Y_6WO_{12}, and Yb_6WO_{12} can be treated as insulators. It was revealed that the κ values of Y_6UO_{12} was intermediate between those of Y_6WO_{12} and Yb_6WO_{12} in the whole temperature range.

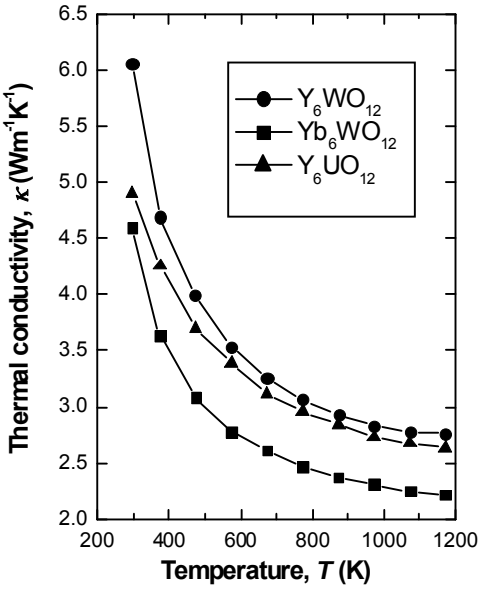

Fig. 1. Temperature dependence of thermal conductivity (κ) of Y_6UO_{12}, Y_6WO_{12}, and Yb_6WO_{12} [3].

REFERENCES

[1] Y. Zheng *et al.*, "Thermal conductivity of Y_6WO_{12}, and Yb_6WO_{12} ceramics," *J. Nucl. Mater.*, **419** (2011) 357.
[2] S. F. Bartram, "Crystal structure of the rhombohedral $MO_3R_2O_3$ compounds (M = U, W, or Mo) and their rela-tion to ordered R_7O_{12} phases," *Inorg. Chem.*, **5** (1966) 749.
[3] Y. Zheng et al., "Synthesis and thermal conductivity of Y_6UO_{12}," *J. Nucl. Sci. Technol.*, **48** (2012) 526.
[4] B. Schulz, *High Temp. High Press.*, **13** (1988) 649.

採択課題番号 25P1-15　アクチニド含有酸化物の物性に関する基礎研究　　プロジェクト
（阪大・工）山中伸介、黒崎　健、牟田浩明、大石佑治

PR1-16 Measurements of Neutron Capture Cross Sections for Radioactive Nuclei

S. Nakamura, K. Terada
T. Fujii[1], A. Uehara[1] and H. Yamana[1]

Japan Atomic Energy Agency
[1]Research Reactor Institute, Kyoto University

INTRODUCTION: A series of experiments with an activation method has been performed to measure thermal-neutron capture cross-sections and resonance integrals of Minor Actinides (MAs), *ex.*^{237}Np, ^{241}Am and so on. Americium-243 is one of the important MAs, because it has long half-life (7370yr) and products higher Cm isotopes *via* neutron capture reaction, *i.e.* ^{244}Cm, ^{245}Cm, and ^{246}Cm. However, there still exist large discrepancies among reported data of the thermal-neutron capture cross-section (σ_0). So, the re-measurement of σ_0 for ^{243}Am have been performed. In our previous experiment, we found that the possibility that the emission probabilities of gamma rays for ^{244g}Am would be improved greatly from 30% error to a few %. Then, the measurement for the neutron capture cross-section of the ^{243}Am(n,γ) reaction was done again together with re-measuring the γ-ray emission probabilities.

EXPERIMENTS: The amount of a high-purity ^{243}Am standardized solution was measured with an alpha spectrometer, EG&G ORTEC SOLOIST alpha spectrometer. **Figure 1** shows an example of an α-ray spectrum for the ^{243}Am standard solution

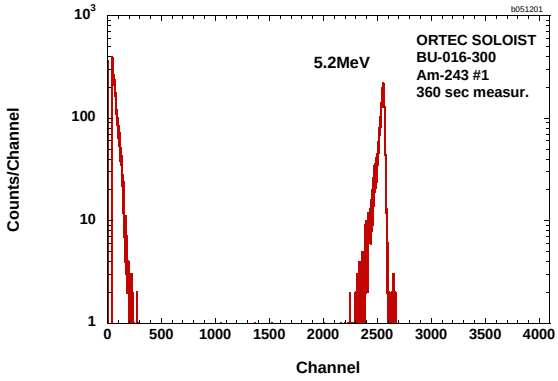

Fig.1 An alpha-ray spectrum obtained for the ^{243}Am standard solution. 5.2MeV α-ray peak was clearly observed.

The detection efficiency was measured with an ^{241}Am checking source (142.9 α/sec). Its specific activity was estimated as 500Bq/μl. So, 2μl(1,000Bq) of the solution was pipetted and dropped on a high purity quartz plate, which was 10mm in width, 30mm in length, and 2mm in thickness. The quartz plate was dried by an infrared lamp, and then the amount of ^{243}Am was measured by the alpha spectrometer. The plate covered with an acrylic plate, and then wrapped doubly with vinyl bags. The irradiation for the ^{243}Am target was performed for10 min at the Pn-2 of the KUR in 1MW power operation. Pieces of Au/Al and Co/Al alloy wires were irradiated together with the Am sample to monitor neutron flux components at the irradiation position. A high-purity Ge detector was used to measure the γ rays emitted from the Am sample and wires to obtain their induced activities. The γ-ray measurement was performed about 2 hours later from the end of the irradiation. **Figure 2** shows an example of γ-ray spectrum of ^{243}Am sample.

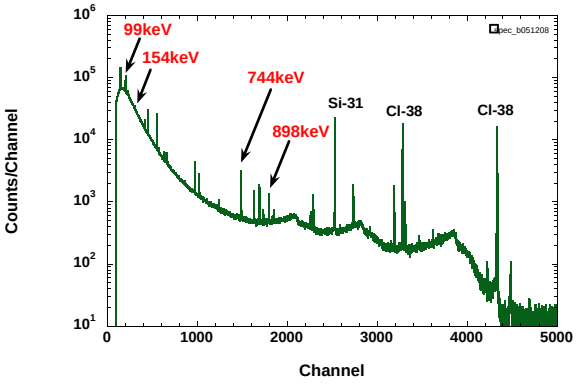

Fig.2 An example of γ-ray spectrum of ^{243}Am sample

Decay γ rays emitted from ^{244g}Am (10.1h) were clearly observed at the energies of 154, 744 and 898 keV. The 99-keV γ-ray is due to the ^{243}Am. The same irradiations and measurements were repeated three times, and therefore the sufficient statistics were obtained.

ANALYSIS: The ^{244g}Am ground state decays to the 6^+ state of ^{244}Cm by the probability of 100% via β^- decay, and there is no transition from the ^{244m}Am isomer to ground states of ^{244}Am. Utilizing this decay scheme, emission probabilities of γ-rays emitted from ^{244g}Am could be derived straightforward form the ratios of γ-ray yields for 154, 744 and 898 keV. If the emission probabilities of γ-rays can be derived, the cross section of ^{243}Am(n,γ)^{244g}Am reaction would be derived.

Data analysis is now in progress.

採択課題番号 25P1-16　　放射化法による長寿命核種の中性子断面積研究　　プロジェクト
（原子力機構）　中村詔司、寺田和司
（京大・原子炉）藤井俊行、上原章寛、山名　元